Pol. J. Environ. Stud. Vol. 35, No. 3 (2026), 3055-3067
DOI: *10.15244/pjoes/203768* ONLINE PUBLICATION DATE: 2025-06-04

Original Research

Effect of Freeze-Thaw Cyclic Aging on the Adsorption Performance of Sheep Manure Biochar

Jiao Chen[1, 2, 3], Rui Li[1], Aiping Zhang[2], Jiayi Liu[1], Yi Tang[1], Zhipeng Zhang[3], Yixin Lu[1, 2, 3]*

[1]School of Materials and Environmental Engineering, Chengdu Technological University, Chengdu 611730, China
[2]Sichuan Environmental Protection Key Laboratory of Persistent Pollutant Wastewater Treatment, Chengdu 610066, China
[3]Engineering & Technology Center of Groundwater Pollution Control for Environmental Protection in Sichuan, Chengdu 610081, China

Received: 04 March 2025
Accepted: 06 April 2025

Abstract

Biochar, SMB, was prepared from waste sheep manure and aged under simulated freeze-thaw cyclic conditions, and the effects of freeze-thaw cyclic aging on the performance and behavioral features of SMB when adsorbing methylene blue (MB) dye in water and its influence mechanism were investigated. The results showed that 7~42 cycles of freeze-thaw aging could effectively improve the pore structure of SMB and enhance its adsorption performance. After 14 freeze-thaw cycles, SMB could remove 95.7% of MB under the optimal operating conditions, and the adsorption amount of MB reached 143.5 mg/g, which was 14% higher than that of unaged SMB. When the freeze-thaw cycles reached 49, the pore structure of SMB was damaged, and its adsorption performance deteriorated, and the adsorption amount of MB was 18.8% lower than that before aging. The adsorption behaviors of SMB on MB both before and after freeze-thaw cyclic aging were chemically dominated, multilayered, entropy-driven, spontaneous, and heat-absorbing. Freeze-thaw cyclic aging increased the chemical dominance and spontaneity of adsorption in the shorter term, while decreasing them in the longer term. The adsorption mechanisms all involved electrostatic attraction, pore filling, hydrogen bonding, and π-π bonding interaction, with pore filling being enhanced after shorter-term freeze-thaw cyclic aging. The findings provide broader theoretical support for the application and promotion of SMB in actual pollution management.

Keywords: freeze-thaw cyclic aging, sheep manure biochar, methylene blue, adsorption

Introduction

Biochar, as a popular novel multifunctional material recently, is a carbon-rich solid produced via thermolysis of biomass utilizing high-temperature facilities under adiabatic or anoxic environments [1]. Biochar has demonstrated tremendous advantages and potential in sewage disposal [2-4], soil remediation

*e-mail: yxlu61@163.com
Tel.: +86-159-286-28507
Fax: +86-028-879-92337

[5], greenhouse gas emission reduction [6], ecological restoration [7], etc., and has been extensively applied in the contaminated environment protection areas. Usually, biochar using waste biomass as rough material, such as agricultural and forestry waste [8], domestic waste biomass [9], municipal residual sludge [10], etc., can not only ease the tension of waste disposal and solve the issue of pollution arising from arbitrary discharge of waste, but also provide more optional solutions for the management of environmental contamination and the utilization of waste resources.

Currently, a growing number of innovative abandoned biomass feedstocks have been exploited and used for the preparation of biochar, among which the research on biochar from livestock and poultry manure has been increasing [11]. Sheep farming, for example, produces a large amount of sheep manure waste every year, and there are inherent nitrogen elements and a large number of pathogenic microorganisms in the untreated sheep manure, which can cause extensive pollution of the agricultural environment or eutrophication of water bodies and other problems if it is arbitrarily discharged into the environment [12]. At present, the most commonly used traditional handling method for sheep manure is to process it into organic fertilizer, but the application of sheep manure also brings many side effects, such as infectious pests and diseases, fermentation and seedling burning, toxic gas hazards, slow fertilizer effect, etc., and the residual heavy metals and hormones contained in the sheep manure may also bring hidden dangers to the food safety and the sustainable development of the plantation industry [13]. To address the issue of sheep manure pollution, the process of preparing sheep manure into biochar for reuse has become a green and resourceful approach to the utilization of sheep manure recently, which exerts an essential and positive significance on environmental protection and the sustainable development of the farming industry.

Existing reports concerning sheep manure biochar have mostly centered on its adsorption application and effect upgrading of pollutants such as herbicides [14], nonsteroidal anti-inflammatory drug [15], organic dyes [16], nitrogen and phosphorus nutrients [17], and heavy metals [18] in water, whereas little care has been placed on the study of its adsorption performance as affected by the actual environment. Indeed, once biochar enters the environment, it may undergo aging due to physical, chemical, or biological effects over time or environmental conditions, leading to changes in its physicochemical properties, which may in turn alter its adsorption of pollutants or affect the migration of pollutants in the environmental medium [19]. At present, the research on the effect of aging on biochar is still in the exploratory stage. The aging process of biochar after entering the environment is extremely complex, and the types mainly include natural aging, high-temperature aging, freeze-thaw cyclic aging, and oxidative aging [20]. Among them, the freeze-thaw cycle refers to the common situation of alternating freezing and thawing processes in the environment, and the occurrence of a freeze-thaw cycle in water bodies and soil environments is a relatively common phenomenon due to the influence of seasons and geographical locations [21]. When freeze-thaw cycles occur, they will have a direct impact on the biochar in the medium [22]. Different types of biochar will show differences when facing environmental aging, and the effects of various types of aging on the structure and adsorption properties of biochar and the mechanisms of the effects need to be further explored. However, studies on the effects of aging on the adsorption of pollutants in water by sheep manure biochar have not yet been reported, and the mechanism of its influence is not yet clear.

Therefore, in this paper, the freeze-thaw cycle was selected as the aging method of biochar, and waste sheep manure was used as the raw material to prepare biochar and adsorb methylene blue (MB), a typical organic dye in water, to investigate the changes of adsorption performance of sheep manure biochar before and after being affected by freeze-thaw cyclic aging and analyze its influence mechanism, aiming to provide scientific guidance for the effective application of sheep manure biochar in real polluted environments.

Materials and Methods

Main Reagents and Solutions

The main reagents available for the experiments included NaOH, HCl, $C_{16}H_{24}ClN_3O_3S$, etc. A 1000 mg/L MB masterbatch solution was made and diluted for batch experiments. The 1 mol/L HCl solution and NaOH solution were made for the initial pH adjustment of the solution; the HCl solution was also utilized for the acid washing of the biochar. The reagents were analytically pure, and the water used was deionized water.

Preparation and Aging of Biochar

Preparation of sheep manure biochar: To obtain good biochar structure and properties, based on the characteristics of sheep manure biomass and previous experimental experience, the oxygen-limited pyrolysis method was selected to prepare biochar in this study. The collected waste sheep manure was dried, crushed, and loaded into a ceramic crucible, compacted and covered, and sent into a high-temperature box-type resistance furnace with a continuous flow of nitrogen gas to create an oxygen-limited atmosphere. It was heated to 500 °C with a temperature gradient of 5 °C/min, then to 700 °C with a temperature gradient of 10 °C/min, and then kept at a constant temperature for 2 h. After pyrolysis, 25 mL of HCl solution was added to each 1 g of pyrolysis product, and placed in a constant temperature oscillator at 25 °C and oscillated at a rotational speed of 150 r/min for 30 min. After acid washing, the pyrolysis

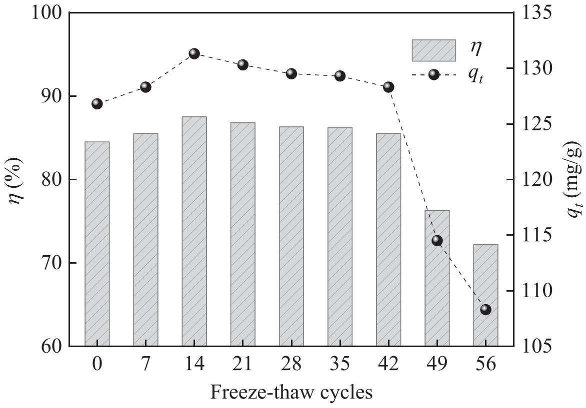

Fig. 1. MB removal effect under different freeze-thaw cycles.

product was washed several times until the pH of the supernatant stabilized. The filter residue was dried and passed through a 100-mesh sieve, and the sieve output with a particle size of less than 150 μm was sheep manure biochar, labeled SMB.

Aging of SMB: The freeze-thaw cycle method was used. The SMB was placed in a centrifuge tube, and an appropriate amount of deionized water was added. To simulate the conventional freeze-thaw environment and to ensure that the biochar samples were completely wetted, the solid-liquid ratio (*m*:*V*) of SMB to deionized water was 1:4. The centrifuge tubes were sealed and placed in a refrigerated freezer for 12 h at -20 ℃, and then taken out and thawed at 25 ℃ for 12 h. One freeze-thaw cycle was completed every day, and the samples were removed and dried after 7, 14, 21, 28, 35, 42, 49, and 56 cycles, respectively, to obtain the freeze-thaw cycle-aged SMB (SMB-FT), which was labeled as SMB-FT7, SMB-FT14, SMB-FT21, SMB-FT28, SMB-FT35, SMB-FT42, SMB-FT49, and SMB-FT56, respectively.

Adsorption Experiment Program

A series of 250 mL conical flasks was prepared, 100 mL of MB solution with a mass concentration of 60 mg/L was added, and 0.04 g of SMB or SMB-FT was added, and the flasks were shaken at a constant rate of 180 r/min for 240 min in a 25 ℃ gas-bath constant-temperature oscillator. After standing for 5 min, the supernatant was filtered through a 0.45 μm filter membrane, and the filtrate was collected to detect the remaining MB mass concentration. The SMBs were screened under specific freeze-thaw cycles to further investigate the adsorption influences, including the effects of initial solution pH values (3~11), SMB dosage (0.1~0.65 g/L), oscillation time (0~480 min), initial MB concentration (40~180 mg/L), and reaction temperature (25~45 ℃).

Analytical Methods

Characterization of biochar: Surface morphology was analyzed with ZEISS Gemini 300 Field Emission Scanning Electron Microscope; Specific surface area (SSA), total pore volume (TPV) and average pore diameter (APD) were analyzed with ASAP2460 Automatic Specific Surface and Porosity Analyzer; Changes in surface functional groups were analyzed with Thermo Scientific Nicolet 6700 Fourier infrared spectrometer.

MB mass concentration analysis: Visible spectrophotometry was used, with a maximum absorption wavelength of 665 nm. The removal rate (η, %) and adsorption amount (q_t, mg/g) of MB were calculated using Eq. (1) and Eq. (2), respectively, by taking the average value after repeating each experiment three times.

$$\eta = \frac{C_0 - C_t}{C_0} \times 100\% \tag{1}$$

$$q_t = \frac{(C_0 - C_t)V}{m} \tag{2}$$

where C_0 and C_t denote the original MB mass concentration and the residual MB mass concentration (mg/L) in the water after *t* min of oscillation reaction, respectively; *V* denotes the amount of water intake (mL); and *m* denotes the amount of SMB or SMB-FT dosed (g).

Results and Discussion

Effect of Freeze-Thaw Cycles on Adsorption

The effect of freeze-thaw cycles on the adsorption performance of SMB is shown in Fig. 1. After 7~42 freeze-thaw cycles, the removal effect of MB was enhanced. The η and q_t values of SMB-FT14-treated MB reached the maximum of 87.5% and 131.3 mg/g, respectively, which were 3% and 4.5 mg/g higher than those of the unaged SMB. When the freeze-thaw cycles reached 49, the η and q_t values were reduced by 8.2%

and 12.3 mg/g, respectively, compared to pre-aging, and even more at 56 freeze-thaw cycles of aging.

It was seen that shorter-term freeze-thaw cyclic aging enhanced the adsorption properties of SMB, while it acted inversely in the longer term [23]. The structure of the SMB after 14 freeze-thaw cycles was most favorable for MB removal, while the structure of the SMB after 49 freeze-thaw cycles began to suffer more damage [24]. To further explore the adsorption performance of SMB after aging by freeze-thaw cycles, the unaged SMB, SMB-FT14, and SMB-FT49 were selected as typical representatives for subsequent experimental studies.

Analysis of Adsorption Affecting Factors

Effect of Initial Solution pH

Fig. 2a) shows the removal status of MB in water by SMB, SMB-FT14, and SMB-FT49 when the initial solution pH was from 3 to 11. The η and q_t values increased with the upward increase of the initial solution pH. The best MB removal effect was achieved when the initial solution pH was 11, where the η values were 89.7%, 95.7%, and 81.2%, and the q_t values were 134.5, 143.5, and 121.8 mg/g, respectively. Of these, SMB-FT14 exhibited the best adsorption performance. In this study, the adsorbent MB was mainly in cationic form, and in acidic environment, the surface functional groups of SMBs showed a high degree of protonation [25], which was not easy to have electrostatic attraction effect with MB cations, and H^+ competed for adsorption sites with MB cations, resulting in poor adsorption effect [26]. In the alkaline environment, the surface functional groups of the three biochars were deprotonated, the surface negative charge was enhanced, and the electrostatic gravitational effect on MB cations was enhanced, thus augmenting the adsorption effect [27].

Effect of Biochar Dosage

Fig. 2b) reflects the removal of MB in water when the dosage of SMB, SMB-FT14, and SMB-FT49 was 0.1~0.65 g/L. When the dosage of the three biochars increased from 0.1 g/L to 0.65 g/L, the corresponding η values rose by 65.3, 50.9, and 72.8 percentage points, respectively, whereas the q_t values decreased by 113, 202, and 63.1 mg/g, respectively. The adsorption sites increased or even exceeded when the dosage of SMB, SMB-FT14, and SMB-FT49 was larger, and the efficiency of removing MB was higher, but the amount of MB removed per unit mass of the three biochars decreased [28]. Therefore, considering the removal effect of MB and the cost of biochar dosing, 0.45 g/L, 0.4 g/L, and 0.55 g/L were selected as the respective optimal dosages for SMB, SMB-FT14, and SMB-FT49, and their η and q_t values reached over 93% and 100 mg/g, respectively. SMB-FT14 displayed the optimal adsorption capacity at the lowest dosage, confirming that the appropriate cycles of freeze-thaw aging would not destroy the structure of the biochar, but rather facilitated the enhancement of its adsorption performance [29]. However, when the number of freeze-thaw cycles reached or exceeded 49, the adsorption capacity of SMB was significantly weakened.

Effect of Oscillation Time

The conditions of MB removal by SMB, SMB-FT14, and SMB-FT49 at different oscillation times (0~480 min) are shown in Fig. 2c). In the range of 240 min, the increasing trend of MB removal effect with the increase of the oscillation time was more obvious, while this increasing trend slowed down after that. Therefore, the optimum oscillation time was 240 min, when MB was removed by SMB, SMB-FT14, and SMB-FT49 with η values of 94.4%, 95.7%, and 93.7%, and q_t values of 125.9, 143.5, and 102.2 mg/g, respectively. In terms of the level of pollutant removal per unit mass of biochar, the SMB-FT14 possessed the highest MB adsorption, and the q_t values increased by 14% and 40.4% compared to SMB and SMB-FT49, respectively, while the q_t value of SMB-FT49 decreased by 18.8% compared to SMB. The whole adsorption process consisted of fast adsorption (I, 0~90 min), slow diffusion (II, 90~240 min), and adsorption equilibrium (III, 240~480 min) stages. In stage I, the adsorption rate was high, and the adsorption amount rose rapidly. In stage II, the adsorption rate decreased with the decrease of MB concentration in the solution and the decrease of adsorption sites on the three kinds of biochar, and the growth of MB removal effect slowed down [30], and the adsorption basically reached the equilibrium after 240 min, and then entered into stage III, where the adsorption process was basically completed [31].

Effect of Initial MB Concentration

Fig. 2d) demonstrates the removal of MB from water by SMB, SMB-FT14, and SMB-FT49 when the initial MB concentration was 40~180 mg/L. The η (q_t) values of the three biochars in removing MB decreased (increased) with the increasing initial MB concentration. In the MB solution with low initial concentration, the content of MB was limited, and the adsorption sites provided by biochar were relatively rich, so it was able to maximize the removal of MB in the solution [32]. When the initial concentration of the MB solution was high, the adsorption sites provided by biochar became limited, and they were all consumed, and the adsorption amount of MB by biochar reached the maximum. However, a large amount of unfixed MB remained in the solution, resulting in a relatively low removal rate [33].

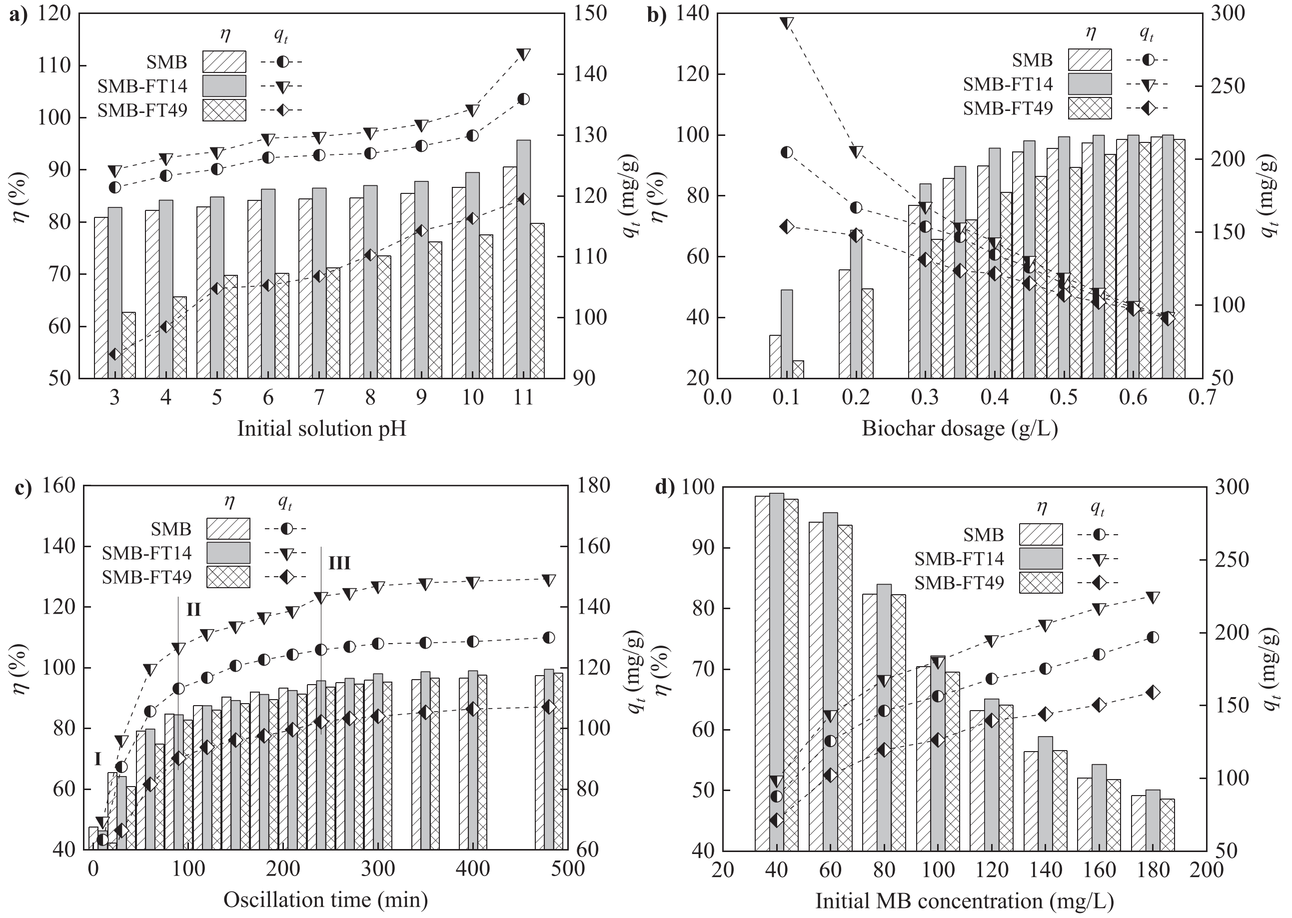

Fig. 2. MB removal effect under different a) initial solution pH, b) biochar dosage, c) oscillation time, and d) initial MB concentration.

Adsorption Behavioral Characteristics of Aged SMBs

Dynamic Characteristics

Dynamic fittings for MB adsorption were carried out by Origin 9.0 software based on the quasi first order dynamic (QFOD) model (Eq. 3), the quasi second order dynamic (QSOD) model (Eq. 4), the Weber-Morris dynamic (WMD) model (Eq. 5) and the Elovich dynamic (ED) model (Eq. 6). The results are shown in Fig. 3 and Table 1.

$$\ln(q_e - q_t) = \ln q_e - k_1 t \tag{3}$$

$$\frac{t}{q_t} = \frac{t}{q_e} + \frac{1}{k_2 q_e^2} \tag{4}$$

$$q_t = k_3 t^{0.5} + A \tag{5}$$

$$q_t = k_4 \ln t + B \tag{6}$$

where q_e and q_t denote the equilibrium adsorption amount of MB (mg/g) and the adsorption amount of MB at oscillation t min (mg/g), respectively; k_1, k_2, k_3, and k_4 denote the rate constants of dynamic models (3)~(6), with units of min^{-1}, g/(mg·min), mg/(g·$min^{0.5}$) and mg/(g·min), respectively; *A* and *B* denote the empirical constants.

As can be seen from Fig. 3 and Table 1, the adsorption dynamic characteristics of SMB, SMB-FT14, and SMB-FT49 on MB were better affixed to the QSOD model, and their correlation coefficients, R^2, reached 0.9707~0.9807, which were significantly higher compared with those of the other models, and the theoretical and experimental values of q_e were close. Thus, it is evident that the adsorption behavior was chemically dominated, and freeze-thaw cyclic aging did not erase this property when SMB adsorbed MB. The q_t values increased significantly with the increase of the oscillation time and then leveled off, and the adsorption rate decreased with the increase of the oscillation time, which indicated that the external diffusion and the internal diffusion played major roles in the adsorption of MB [34]. In addition, the fitted line of the WMD model did not pass through the origin, suggesting that intra-particle diffusion was not the only rate-controlling step in MB removal, but rather acted in conjunction with the other adsorption stages [35], including the external mass transfer process, which also equally affected the final MB adsorption rate.

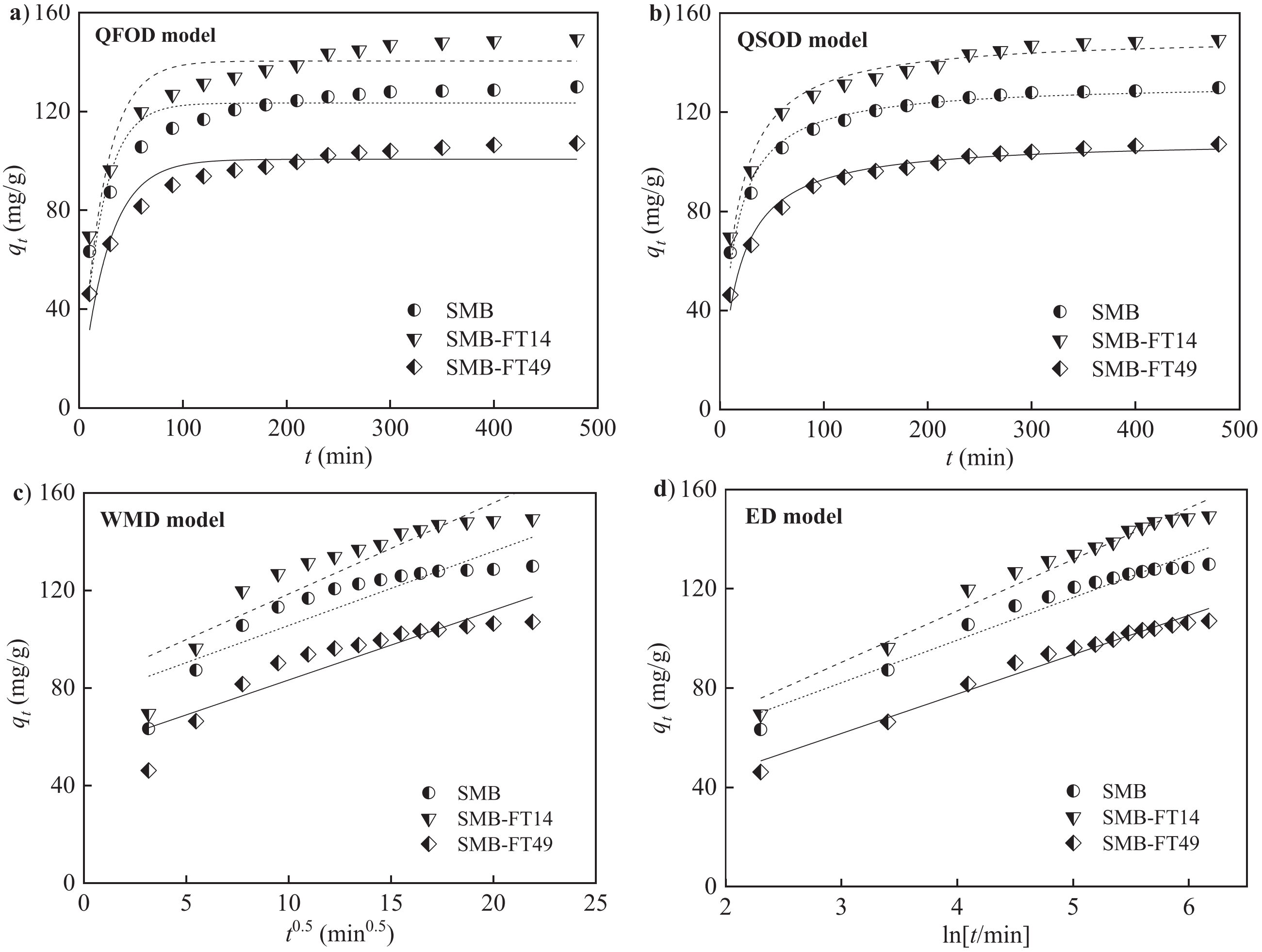

Fig. 3. Adsorption dynamic fitting results of SMB, SMB-FT14, SMB-FT49 for MB: a) QFOD model, b) QSOD model, c) WMD model, and d) ED model.

Isothermal Characterization

The Langmuir, Freundlich, and Temkin models shown in Eqs. (7), (8), and (9), respectively, were used for isotherm fitting in this study. The results are shown in Fig. 4 and Table 2.

$$q_e = \frac{q_m K_L C_e}{1 + K_L C_e} \quad (7)$$

$$q_e = K_F C_e^{1/n} \quad (8)$$

$$q_e = K_T \ln C_e + C \quad (9)$$

where q_e and q_m denote the equilibrium adsorption amount and theoretical maximum adsorption amount of MB, respectively, mg/g; C_e denotes the MB concentration at adsorption equilibrium, mg/L; K_L denotes the constant of model (7), L/mg; K_F and n denote the constants of model (8); K_T and C denote the constants of model (9).

It can be seen that the R^2 values of the three biochars fitted with the Freundlich model at different reaction temperatures exceeded 0.97, indicating that the isothermal adsorption characteristics were more in line with the connotation of the Freundlich model. Their adsorption behaviors were dominated by the adsorption of the multimolecular layer [36].

In the Freundlich model, the values of $1/n$ and K_F can reflect the ease or difficulty of adsorption occurrence and the strength of performance, respectively [37]. The value of $1/n$ in the range of 0.1~1.0 indicates that the adsorption behavior is easy to occur, and the smaller the value of $1/n$ in this value range, the easier the adsorption occurs, while the value of $1/n$ over 1.0 indicates that the adsorption behavior is relatively difficult to occur [38]. The analysis demonstrated that the mean values of $1/n$ corresponding to SMB, SMB-FT14, and SMB-FT49 were 0.1582, 0.1450, and 0.1673, respectively, indicating that their adsorption behaviors on MB were all easy to occur. However, at the same reaction temperature, SMB-FT14 presented the lowest value of $1/n$, indicating that its adsorption behavior was easier compared to that of SMB, whereas SMB-FT49 behaved in the opposite way.

Table 1. Fitting parameters of the adsorption dynamic models.

Dynamic model	Parameter	SMB	SMB-FT14	SMB-FT49
QFOD	q_e	123.4	140.4	100.6
	k_1	0.0483	0.0442	0.0376
	R^2	0.8426	0.8307	0.8586
QSOD	q_e	131.8	150.9	108.9
	k_2	0.00058	0.00045	0.00053
	R^2	0.9807	0.9707	0.9787
WMD	A	75.2	81.1	54.7
	k_3	3.0415	3.7365	2.8610
	R^2	0.7601	0.8029	0.8061
ED	B	30.7	28.2	14.2
	k_4	17.1489	20.7248	15.8646
	R^2	0.9491	0.9667	0.9697

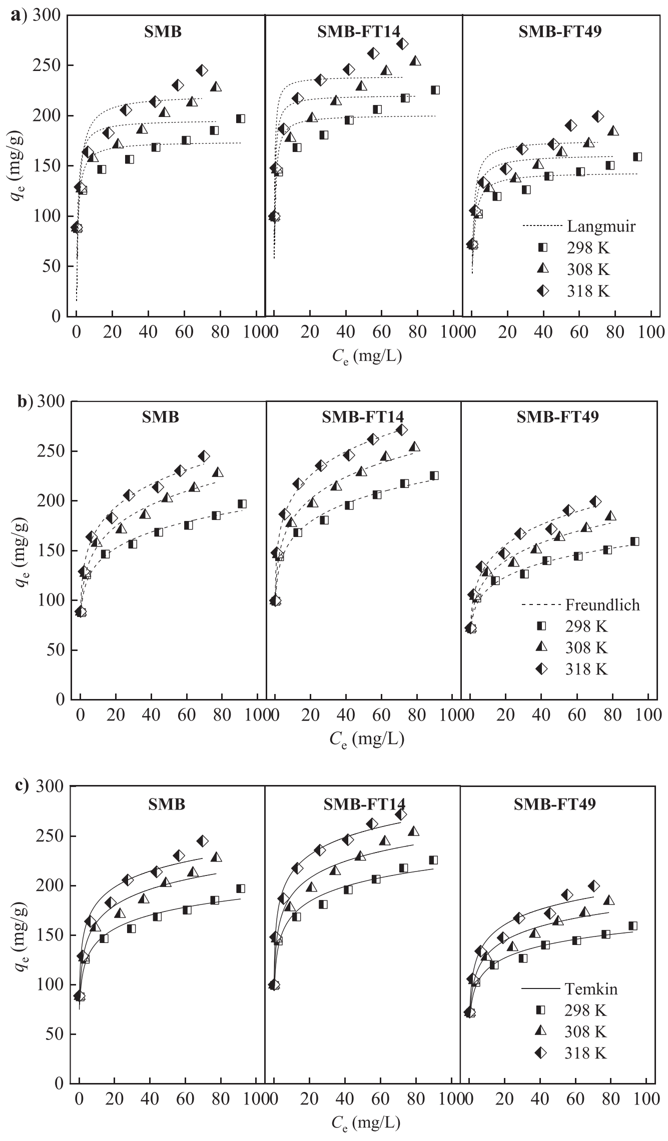

Fig. 4. Adsorption isothermal fitting results of SMB, SMB-FT14, SMB-FT49 for MB: a) Langmuir model, b) Freundlich model, and c) Temkin model.

Table 2. Fitting parameters of the adsorption isothermal models.

Biochars	T (K)	Langmuir model			Freundlich model			Temkin model		
		q_m	K_L	R^2	$1/n$	K_F	R^2	C	K_T	R^2
SMB	298	174.3	1.2247	0.7717	0.1458	98.4685	0.9779	96.7777	19.8654	0.9706
	308	195.8	1.3941	0.6656	0.1674	105.6928	0.9835	108.3622	23.8191	0.9526
	318	220.9	0.7674	0.5695	0.1613	119.5482	0.9865	128.4424	23.3229	0.9386
SMB-FT14	298	200.7	1.7541	0.7592	0.1399	117.7788	0.9804	118.0509	21.8579	0.9717
	308	220.3	2.4149	0.6947	0.1504	128.5777	0.9882	133.1593	24.6244	0.9663
	318	238.9	3.1903	0.7091	0.1447	146.2788	0.9959	152.8571	25.8348	0.9878
SMB-FT49	298	143.9	0.9076	0.8152	0.1521	78.3306	0.9781	75.3632	17.1439	0.9769
	308	161.6	0.9347	0.7536	0.1739	83.0634	0.9802	82.3094	20.6561	0.9615
	318	175.8	1.0796	0.7486	0.1760	91.9989	0.9809	93.5463	22.2679	0.9634

Table 3. Fitting parameters of adsorption thermodynamics.

Biochars	ΔG			ΔH	ΔS	R^2
	298 K	308 K	318 K			
SMB	-8.8697	-9.7702	-11.0138	23.1329	0.1072	0.9829
SMB-FT14	-10.0386	-11.5581	-13.4861	41.3958	0.1724	0.9907
SMB-FT49	-8.1556	-9.2564	-10.6234	28.6589	0.1234	0.9923

A larger K_F value implied a greater adsorption strength and a better adsorption performance [39]. In this study, the K_F value of SMB-FT14 was the largest, while that of SMB-FT49 was the smallest, reflecting the strong and weak order of their adsorption capacity of MB in the following order: SMB-FT14>SMB>SMB-FT49. Shorter-term freeze-thaw cyclic aging improved the adsorption properties of SMB and made the adsorption behavior more likely to occur, whereas longer-term freeze-thaw cyclic aging was detrimental to the adsorption of MB.

Thermodynamic Characterization

The experimental data of adsorption of SMB, SMB-FT14, and SMB-FT49 on MB in water at different reaction temperatures were thermodynamically analyzed according to Eqs. (10) and (11). The fitting results are shown in Table 3.

$$\Delta G = -8.314 T \ln K_e \quad (10)$$

$$\Delta G = \Delta H - T\Delta S \quad (11)$$

where ΔG, ΔH, and ΔS denote the Gibbs free energy change, enthalpy change, and entropy change, with units of kJ/mol, kJ/mol, and kJ/(mol·K), respectively; K_e denotes the equilibrium constant, which is calculated from the ratio of q_e to C_e.

The ΔG values of the three biochars were negative at different reaction temperatures, indicating that their adsorption behavior on MB was spontaneous [40]. The larger absolute value of ΔG indicates the stronger adsorption driving force. Comparatively, the absolute value of ΔG was the largest for SMB-FT14, followed by SMB, and the smallest for SMB-FT49, indicating that the adsorption of MB by SMB-FT14 was the most spontaneous, and the higher the reaction temperature was, the more obvious was the tendency of spontaneous adsorption proceeding, which illustrated that the appropriate elevation of the reaction temperature promoted the spontaneous proceeding of adsorption reaction, and thus the adsorption capacity of SMB was enhanced [41]. The value of ΔH was greater than 0, indicating that the adsorption process was a heat-absorbing reaction, and the elevated temperature was favorable to the adsorption. The ΔH values were all above 20.9 kJ/mol, showing that chemisorption was the primary mode of action [42], regardless of whether or not freeze-thaw cyclic aging was applied to SMB. The ΔH value of SMB-FT14 showed the largest, followed by SMB-FT49, and the smallest for SMB, which revealed that the chemically dominant adsorption behaviors of SMB aged by freeze-thaw cycles were stronger, and the shorter-term freeze-thaw cyclic aging was more beneficial to the enhancement of chemisorption. Tan *et al.* [43] pointed out that the dominant forces of adsorption were van der Waals, dipole, and hydrogen bonding forces when the ΔH values were 4~10, 2~29, and 2~40 kJ/mol, respectively. It was hypothesized

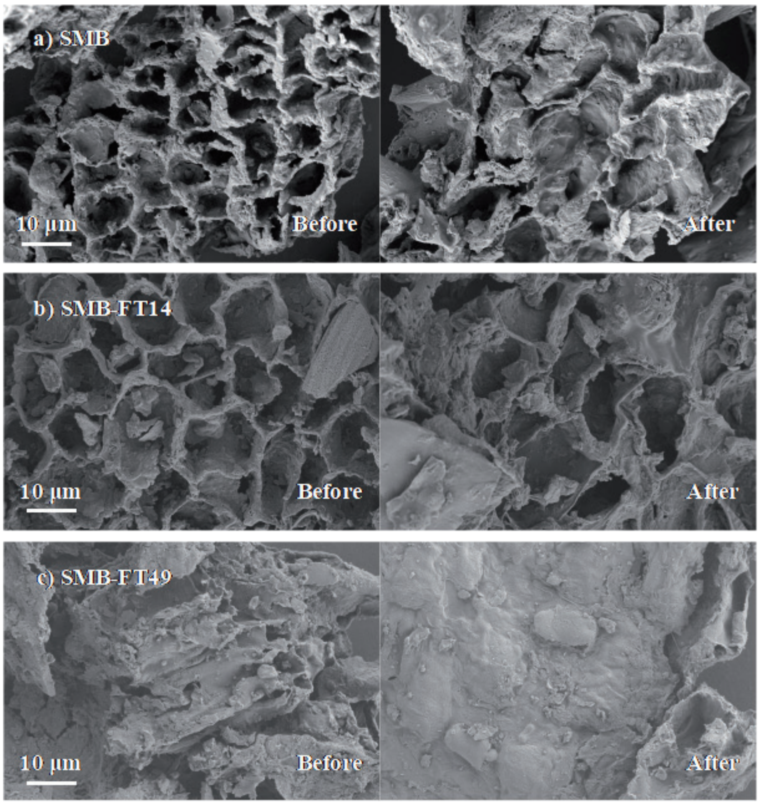

Fig. 5. SEM analysis results of a) SMB, b) SMB-FT14, and c) SMB-FT49 before and after MB adsorption.

that there was also an obvious hydrogen bonding force driving the adsorption behavior of SMB or SMB-FT on MB. In addition, the Δ*S* values were above 0, showing that the process of MB adsorption by the three biochars was entropy-driven, and the interfacial disorder of the adsorption process increased.

Adsorption Mechanism Analysis of Aged SMBs

SEM Analysis

Fig. 5 shows the scans of the SMBs before and after MB adsorption under a 4000x electron microscope. The raw SMB exhibited many pore structures, and they were irregularly arranged. The pore size of SMB-FT14 became larger, while the number of pores in SMB-FT49 was significantly reduced. After adsorption of MB, the pores of SMB and SMB-FT49 were heavily filled, while SMB-FT14 also showed many available pores. Therefore, the effects of different freeze-thaw cycles on the surface structure of SMB were distinct.

BET Analysis

Freeze-thaw cyclic aging affects the pore properties of SMB, such as SSA, TPV, and APD, which in turn affects its adsorption capacity. According to the BET analysis results, the SSA value of SMB-FT14 reached 268.5 m^2/g, which increased by 19.7% and 62.2% compared to SMB and SMB-FT49, respectively; the TPV value reached 0.371 cm^3/g, which increased by 20.5% and 87.3% compared to SMB and SMB-FT49, respectively; and the APD value reached 22.15 nm, which was higher than SMB and SMB-FT49 by 39.4% and 68.9%, respectively. The pore properties of SMB-FT14 were superior to those of SMB and SMB-FT49. In contrast, the SSA value of SMB-FT49 decreased by 52.9% and 62.2%, the TPV value decreased by 84.1% and 87.3%, and the APD value decreased by 48.7% and 68.9% compared to SMB and SMB-FT14, respectively, which shows that its pore properties were deteriorated. After MB adsorption, reductions in the values of SSA, TPV, and APD were observed for all three biochars, but the smallest reduction was observed for SMB-FT14.

With the freeze-thaw cyclic aging, SMB was exposed to the freezing-thawing alternating process, the freezing expansion phenomenon occurred, which led to an increase in pore size, the total void space and the number of spots available for adsorption increased, which was more conducive to the pore filling of the MB [44]. However, with the prolongation of the freeze-thaw cyclic aging time, the SMB porosity decreased dramatically, and after excessive freezing and thawing, the pore structure was destroyed due to reaching the tolerance limit, which led to the obvious collapse of the pore structure, and part of the pore structure was blocked, and these changes would be detrimental to the removal of MB by the SMB.

Combined with the adsorption performance and SEM analysis, the shorter-term freeze-thaw cyclic aging

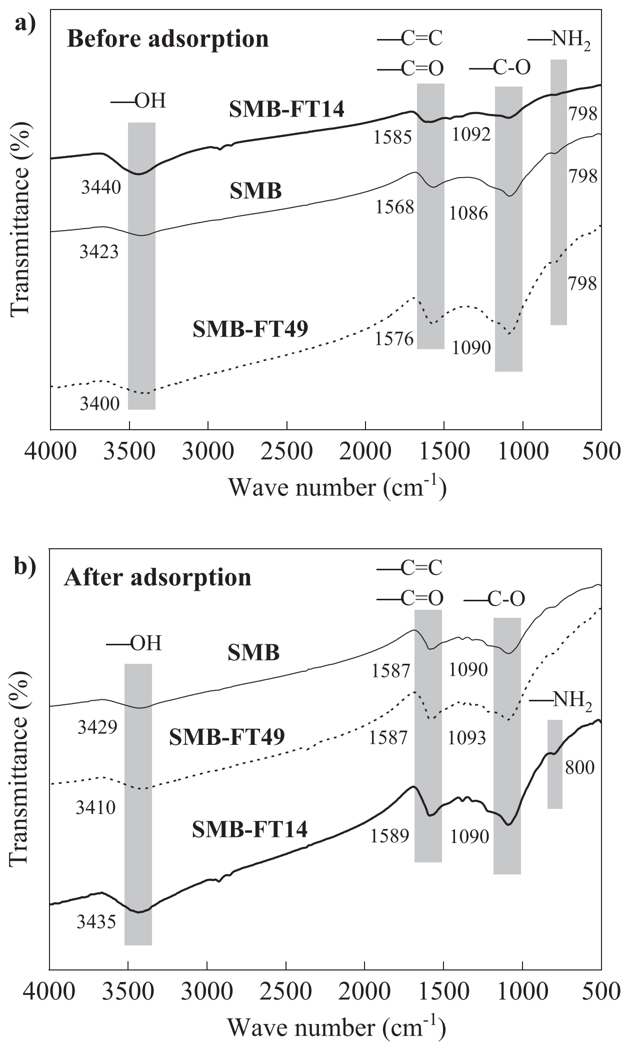

Fig. 6. Comparison of FTIR analysis results of SMB a) before MB adsorption and b) after MB adsorption.

effectively improved the pore properties of SMB, which led to a more perfect structure, thus providing a basis for further enhancement of its adsorption potential, whereas the longer-term aging caused the structure of SMB to rupture or collapse, which negatively affected its adsorption of MB. The fact that the porosity of all three biochars decreased after MB adsorption proved that pore filling was one of the key adsorption mechanisms [45]. SMB-FT14 possessed a richer pore structure than SMB and SMB-FT49, and the remaining space after the end of adsorption was larger, and its excellent structural properties enabled it to have a stronger adsorption performance, whereas SMB-FT49, due to its own underdeveloped pore structure, the pore space at the end of adsorption became less, and most of the pore space had already been filled by MB, which provided a reasonable explanation for the differences in adsorption capacity among the biochars.

FTIR Analysis

Fig. 6 reflects the results of FTIR analysis of SMB, SMB-FT14, and SMB-FT49 before and after MB adsorption. Before adsorption of MB, the surfaces of SMB, SMB-FT14, and SMB-FT49 were distributed with abundant functional group structures, in which the characteristic absorption peaks appearing around 3400, 1600, 1080, and 800 cm^{-1} originated from the —OH, —C=C (—C=O), —C-O, and —NH$_2$ vibrations, respectively. The presence of these functional groups provided favorable conditions for the adsorption of MB [46]. Except for —NH$_2$, the positions of other characteristic peaks on SMB were shifted after undergoing freeze-thaw cycles, indicating that freeze-thaw cyclic aging somehow exerted an influence on the functional groups on SMB, thereby changing the positions of their peaks, which in turn affected the adsorption results.

After adsorption of MB, the positions of the absorption peaks of the above functional groups on SMB, SMB-FT14, and SMB-FT49 were changed to different degrees, indicating that they all participated in the adsorption reaction. The positions of the —OH absorption peaks were shifted to 3429 cm^{-1}, 3435 cm^{-1}, and 3410 cm^{-1}, respectively, suggesting that hydrogen bonding between —OH on biochar and the aromatic ring on MB occurred as one of the vital principles in this adsorption process. The positions of the —C=C and —C=O absorption peaks were shifted to 1587 cm^{-1}, 1589 cm^{-1}, and 1587 cm^{-1}, respectively, which indicated that π-π bonding occurred between the aromatic ring on the biochar and MB, resulting in the change of the position of the telescopic vibration, and thus π-π bonding was also one of the crucial mechanisms for the adsorption process. Hydrogen bonding and π-π bonding interactions play important roles in the adsorption process, which has been reported in a large number of studies [47-49], and the present study confirms the same.

Comprehensively, it is known that the adsorption mechanisms of SMB, SMB-FT14, and SMB-FT49 on MB in water all implicated electrostatic attraction, pore filling, hydrogen bonding, π-π bonding, etc., making it a highly complex process [50]. Although the adhesion mechanism types of SMB, SMB-FT14, and SMB-FT49 on MB in water were basically the same, the pore structure of SMB was affected to different degrees after different cycles of freeze-thaw cyclic aging, and its pore properties showed different degrees of changes, which in turn affected the strength of each mechanism of action in adsorption of pollutants, resulting in the differences in their adsorption effects. Additionally, it is noteworthy that there are differences between the simulated and the real freeze-thaw environments. This is mainly in terms of the range and variation rate of temperature, duration of aging, moisture conditions, other environmental factors such as microbial activity, chemical leaching, and the effect of light. In the actual freeze-thaw cyclic environment, the mechanism by which the adsorption properties of SMB are affected may be more complicated due to the coupling of multiple factors. Therefore, more attention should be given to the influence and mechanism of the above factors on SMB in future research, and the environmental risk assessment of SMB in freeze-thaw environments is also a worthy topic to be explored.

Conclusions

The adsorption effect, adsorption behavioral characteristics, and structural properties of sheep manure biochar (SMB) aged through different periods of freeze-thaw cycles showed variability. The adsorption performance of SMB aged through 14 freeze-thaw cycles was optimized, and its adsorption of MB increased by 14% over that of the raw SMB. The adsorption performance of SMB after 49 freeze-thaw cycles was diminished, and the amount of MB adsorbed decreased by 18.8% over that of the raw SMB. Freeze-thaw cyclic aging reinforced the dominance of chemisorption. Shorter-term freeze-thaw cyclic aging effectively improved the pore structure of SMB to enhance its adsorption performance, while longer-term freeze-thaw cyclic aging showed the opposite effect. Freeze-thaw cyclic aging also altered the strength of the action mechanism, thereby affecting the adsorption capacity of SMB.

Acknowledgments

This study was financially supported by the Open Fund of Sichuan Environmental Protection Key Laboratory of Persistent Pollutant Wastewater Treatment (PPWT2024-02), the Open Fund of Engineering & Technology Center of Groundwater Pollution Control for Environmental Protection in Sichuan (2024-01), the Sichuan Science and Technology Program (2022YFG0307), the Sichuan Student Research Training Program (202511116049), and the CDTU Laboratory Open Fund Program (2024CHZH01).

Conflict of Interest

The authors declare no conflict of interest.

References

1. HARIS M., AMJAD Z., USMAN M., SALEEM A., DYUSSENOVA A., MAHMOOD Z., DINA K., GUO J., WANG W. A review of crop residue-based biochar as an efficient adsorbent to remove trace elements from aquatic systems. Biochar, **6** (1), 47, **2024**.
2. SHARMA R., SHARMA A., MALAVIYA P. Textile wastewater remediation in biochar-amended Phragmites-based horizontal flow constructed wetlands. Journal of Water Process Engineering, **68**, 106550, **2024**.
3. GHOSH S., DAS S., PANJA A., SOLOVCHENKO A., JHA P. Microalgae as potential agents for biochar production: Future of industrial wastewater treatment. Circular Economy, **3** (4), 100117, **2024**.
4. TORBOLI A., FOLADORI P., LU M., Gialanella S., Maines L. Spent coffee ground biochar for phosphate adsorption in water: Influence of pyrolysis temperature and iron-coating activation method. Cleaner Engineering and Technology, **23**, 100839, **2024**.
5. CHANG Y., LIN L., SHEN J., LIN Z., DENG X., SUN W., WU X., WANG Y., LI Y., XU Z. Enhanced nitrogen fixation and Cd passivation in rhizosphere soil by biochar-loaded nitrogen-fixing bacteria: Chemisorption and microbial mechanism. Journal of Hazardous Materials, **481**, 136588, **2025**.
6. CHÁVEZ Á.E., GONZÁLEZ R.A., DÍAZ C.K.A., STÉPHANE GODBOUT S., GÉNÉREUX M., CÔTÉ C., ROUSSEAU N.A., FOURNEL S. Effluent properties and gas emissions from a conventional wintering area and an alternative stand-off pad providing outdoor exercise to dairy cows. Agriculture, Ecosystems and Environment, **380**, 109379, **2025**.
7. LIAO J., HAO G., GUO H., CHEN H. Effects of biochar on plant and microbial communities in landfill soil. Applied Soil Ecology, **204**, 105749, **2024**.
8. SRINADH V.R., REMYA N. Congo red removal using microwave assisted pyrolysis derived magnetic hemp hurd biochar. Chemical Engineering Research and Design, **212**, 321, **2024**.

9. TABANA L., KUPA A., TICHAPONDWA S. Adsorption of hexavalent chromium from wastewater using magnetic biochar derived from peanut hulls. Physics and Chemistry of the Earth, **137**, 103815, **2025**.
10. ZHAO Z. Efficient removal of Cr (VI) containing tunnel wastewater by sludge biochar loaded with ferrous sulfate. Desalination and Water Treatment, **320**, 100786, **2024**.
11. LEE I.J., JANG H.S., KIM C., KANG J.K., LEE G.C., PARK J.S. Evaluation of large-scale poultry manure-derived biochar for efficient cadmium removal in zinc smelter wastewater. Journal of Environmental Management, **370**, 122763, **2024**.
12. WANG J., REN K., ZHANG L. Design and testing of a small-scale composting facility for sheep manure utilizing aeration and thermal treatment. Agriculture, **14** (11), 2070, **2024**.
13. NLEYA Y., YOUNG B., NOORAEE E., BAROUTIAN S. Anaerobic digestion of dairy cow and goat manure: Comparative assessment of biodegradability and greenhouse gas mitigation. Fuel, **381**, 13345, **2025**.
14. LU Y., CHEN J., ZHANG J., FU C. Kinetic, isotherm and thermodynamic studies on the adsorption behavior of atrazine onto sheep manure-derived biochar. Polish Journal of Environmental Studies, **28** (4), 2725, **2019**.
15. MEHMET D.F., MAZLUM Y. Adsorption of naproxen pharmaceutical micropollutant from aqueous solutions on superior activated carbon synthesized from sheep manure: Kinetics, thermodynamics, and mechanism. Journal of Molecular Liquids, **381**, 121839, **2023**.
16. SOUBAI B., CHHAM I.A., SELHAMI B., AKOUIBAA M., ALI S.A.S., FOULANI E.A.A., TAHIRI M. Transforming animal waste into a friendly and economically sustainable adsorbent for removing organic pollutants from aqueous wastewater. Case Studies in Chemical and Environmental Engineering, **10**, 100981, **2024**.
17. FENG Y., ZHAO D., QIU S., HE Q., LUO Y., ZHANG K., SHEN S., WANG F. Adsorption of phosphate in aqueous phase by biochar prepared from sheep manure and modified by oyster shells. ACS Omega, **6** (48), 33046, **2021**.
18. WANG S., LI X., ZHU Y. Comparison of the adsorption capacity and mechanisms of mixed heavy metals in wastewater by sheep manure biochar and Robinia pseudoacacia biochar. Water Science and Technology, **87** (12), 3083, **2023**.
19. LONG X., YU N., LIU W., GAO T., QIU R. A systematic review of biochar aging and the potential eco-environmental risk in heavy metal contaminated soil. Journal of Hazardous Materials, **472**, 134345, **2024**.
20. LIANG J., CHEN X., DUAN X., GU X., ZHAO X., ZHA S., CHEN X. Natural aging and adsorption/desorption behaviors of polyethylene mulch films: Roles of film types and exposure patterns. Journal of Hazardous Materials, **466**, 133588, **2024**.
21. DONG H., WU Z. Effects of freeze-thaw cycles on bioaccessibilities of polycyclic aromatic hydrocarbons. Toxics, **12** (6), 413, **2024**.
22. SHEN J., HUANG G., YAO Y., ZHANG P., ROSENDAHL S. Surface alteration on biochar in long-term application: Insights into pyrolysis, freeze-thaw aging, and dissipation. Surfaces and Interfaces, **46**, 104118, **2024**.
23. ZHU L., CHEN N., ZHANG X., REN L., ZOU R., XIE J., WANG Z., YANG H., HAO Z., QIN J., JIA H. Freeze-thaw cycle events enable the deep disintegration of biochar: Release of dissolved black carbon and its structural-dependent carbon sequestration capacity. Environmental Science & Technology, **58** (47), 20979, **2024**.
24. SHEN J., HUANG G., YAO Y., ZHANG P., ROSENDAHL S. Thermodynamic assessment of Tetrabromobisphenol A (TBBPA) persistence over time in freeze-thaw aged biochar and its environmental significance. Industrial Crops & Products, **221**, 119255, **2024**.
25. LEE H., FIORE S., BERRUTI F. Adsorption of methyl orange and methylene blue on activated biocarbon derived from birchwood pellets. Biomass and Bioenergy, **191**, 107446, **2024**.
26. CHEN X., ZHOU Y., HE J., PILLAI C.S., LI N., XU S., LI J., CHEN X., WANG H. Elevated efficiency in tartrazine removal from wastewater through boron-doped biochar: enhanced adsorption and persulfate activation. Biochar, **6** (1), 79, **2024**.
27. LIAO L., CHEN H., HE C., DODBIBA G., FUJITA T. Boron removal in aqueous solutions using adsorption with sugarcane bagasse biochar and ammonia nanobubbles. Materials, **17** (19), 4895, **2024**.
28. ZHAO T., ALI A., SU J., LIU S., YAN H., XU L. Removal of sulfamethoxazole from water by biosurfactant-modified sludge biochar: Properties and mechanism. Journal of Environmental Chemical Engineering, **12** (6), 114200, **2024**.
29. NAGARAJAN T., FEKERI M.B.H.N., RAJU G., SHANMUGAN S., JEPPU G., WALVEKAR R., RUSTAGI S., KHALID M. Adsorption parameters optimization of spent coffee ground biochar for methylene blue removal using response surface methodology. Chemosphere, **364**, 143242, **2024**.
30. HUANG W., ZHANG M., WANG Y., CHEN J., ZHANG J. Biochars prepared from rabbit manure for the adsorption of rhodamine B and Congo red: characterisation, kinetics, isotherms and thermodynamic studies. Water Science and Technology, **81** (3), 436, **2020**.
31. ZHOU Y., WANG Z., HU W., ZHOU Q., CHEN J. Norfloxacin adsorption by urban green waste biochar: characterization, kinetics, and mechanisms. Environmental Science and Pollution Research, **31** (20), 29088, **2024**.
32. TEWELDEBRIHAN D., DINKA O. Methyl red adsorption from aqueous solution using rumex abyssinicus-derived biochar: Studies of kinetics and isotherm. Water, **16** (16), 2237, **2024**.
33. MASUKU M., NURE F.J., ATAGANA I.H., HLONGWA N., NKAMBULE I.T.T. Pinecone biochar for the Adsorption of chromium (VI) from wastewater: Kinetics, thermodynamics, and adsorbent regeneration. Environmental Research, **258**, 119423, **2024**.
34. WANG F., HOU Y. Adsorption of tricyclazole and 2,4-dichlorophenoxyacetic acid onto biochar produced from anaerobically digested sludge. Water, **16** (18), 2697, **2024**.
35. VELAYUDHAN J., SUBRAMANIAN S. Selenium-doped biochar for removal of anionic acid red and cationic crystal violet dye. Nano, **19** (7), 24500322, **2024**.
36. AFROOZ M., ZEYNALI R., SOLTAN J., MCPHEDRAN N.K. A novel biochar adsorbent for treatment of perfluorooctanoic acid (PFOA) contaminated water: Exploring batch and dynamic adsorption behavior. Journal of Water Process Engineering, **69**, 106586, **2025**.
37. LU Y., CHEN J., ZHAO L., ZHOU Z., QIU C., LI Q. Adsorption of Rhodamine B from aqueous solution by goat manure biochar: kinetics, isotherms, and thermodynamic studies. Polish Journal of Environmental Studies, **29** (4),

2721, **2020**.
38. HUANG W., ZHANG X., TANG Y., LUO J., CHEN J., LU Y., WANG L., LUO Z., ZHANG J. ZVI/biochar derived from amino-modified corncob and its phosphate removal properties in aqueous solution. Journal of Water Process Engineering, **49**, 103026, **2022**.
39. LU Y., LIU Y., LI C., LIU H., LIU H., TANG Y., TANG C., WANG A., WANG C. Adsorption characteristics and mechanism of methylene blue in water by NaOH-modified areca residue biochar. Processes, **10** (12), 2729, **2022**.
40. BABEKER A.M.T., LV S., KHALIL N.M., HAO Z., CHEN Q. Biochar modified by ammonium pyrrolidine dithiocarbamate for high selective adsorption of copper in wastewater. Separation and Purification Technology, **354**, 129436, **2025**.
41. XU C., WANG Y., MA X., WANG X., YANG Y., ZHANG Q. High-efficient removal of tebuconazole from aqueous solutions using P-doped corn straw biochar: Performance, mechanism and application. Bioresource Technology, **412**, 131387, **2024**.
42. CHEN J., TANG C., LI X., SUN J., LIU Y., HUANG W., WANG A., LU Y. Preparation and modification of rape straw biochar and its adsorption characteristics for methylene blue in water. Water, **14** (22), 3761, **2022**.
43. TAN W., LI G., BAI M., YANG M., PENG J., COLIN J.B., YANG W., WANG H. The study of adsorption mechanism of mixed pesticides prometryne-acetochlor in the soil-water system. International Biodeterioration & Biodegradation, **102**, 281, **2015**.
44. WANG L., DOU Z., MA C., JIA X., WANG H., BAO W., WANG L., QU J., ZHANG Y. Remediation of di (2-ethylhexyl) phthalate (DEHP) contaminated black soil by freeze-thaw aging biochar. Journal of Environmental Sciences, **135**, 681, **2024**.
45. PAN X., ZHAO N., SHI H., WANG H., RUAN F., WANG H., FENG Q. Biomass activated carbon derived from golden needle mushroom root for the methylene blue and methyl orange adsorption from wastewater. Industrial Crops & Products, **223**, 120051, **2025**.
46. RAMÍREZ G., CHICA E., CLEMENTE R. Elimination of indigo carmine in water by Pinus patula biochar: Adsorption process optimization, kinetics and isotherms. Journal of Environmental Chemical Engineering, **12** (3), 112425, **2024**.
47. LIU Q., CHANG Q., LIAO X., JIANG Y., LYU X., ZHAO Q., DIAO J., WANG X., HUANG X., LYU S. Adsorption desulphurization performance of biochar that derived from eucalyptus waste. Powder Technology, **448**, 120322, **2024**.
48. LEE G., KIM C., PARK C., RYU G.B., HONG J.H. High-carbon-content biochar from chemical manufacturing plant sludge for effective removal of ciprofloxacin from aqueous media. Chemosphere, **364**, 143118, **2024**.
49. GONG W., QI C., HUANG L., TIAN Z., HUANG Z., TAO C., LIN H., GUO L., YU Z. Adsorption of phosphorus in wastewater by lanthanum-modified magnetic sewage sludge biochar. Desalination and Water Treatment, **320**, 100603, **2024**.
50. PEI N., LUO W., HUANG Q., SUN Y. Adsorption properties of fishbone and fishbone-derived biochar for cadmium in aqueous solution. Agronomy, **14** (11), 2717, **2024**.